

Nonlinear Site Response Analyses and High Frequency Dilation Pulses

G. McAllister & M. Taiebat

*Department of Civil Engineering – University of British Columbia,
Vancouver, BC, Canada*

A. Ghofrani, L. Chen & P. Arduino

Department of Civil and Environmental Engineering – University of Washington, Seattle, WA, USA



*Challenges from North to South
Des défis du Nord au Sud*

ABSTRACT

Nonlinear seismic site response analyses can provide an accurate representation of soil behaviour in response to the propagation of seismic waves. However their use has been limited in conventional engineering practice due to the perceived complexity in parameter selection and usage protocols. Moreover, both total and effective stress nonlinear analyses can be conducted to evaluate seismic site response. It would be insightful from a practical point of view to explore the difference in results when either a total or effective nonlinear analysis is carried out using an advanced soil constitutive model. In this paper, the critical state bounding surface plasticity constitutive model SANISAND is used to investigate the nonlinear response of a thin sand surface layer subjected to seismic loading. The importance of modeling the porous solid-pore fluid interaction is explored and the site response high frequency ground motion is suggested to be caused by dilation pulses during the soil phase transformation process.

RÉSUMÉ

Les analyses de la réponse sismique non linéaire des sites peuvent fournir une représentation précise du comportement du sol en réponse à la propagation des ondes sismiques. Cependant, leur utilisation a été limitée dans la pratique de l'ingénierie conventionnelle à cause de la complexité perçue dans la sélection de paramètres et les protocoles d'utilisation. Par ailleurs, les analyses non linéaires des contraintes totales et effectives peuvent être réalisées pour évaluer la réponse sismique des sites. D'un point de vue pratique, il serait perspicace de comparer la différence entre les résultats des analyses non linéaires totales et effectives en utilisant un modèle constitutif avancé de sol. Dans cet article, le modèle constitutif de l'état critique englobant la plasticité de surface SANISAND, est utilisé pour étudier la réponse non linéaire d'une mince couche de la surface du sable soumise à une charge sismique. L'importance de la modélisation de l'interaction fluide des pores - solide poreux est explorée et la réponse du site, caractérisée par un mouvement de haute fréquence, est suggérée d'être causée par des impulsions de dilatation au cours du processus de transformation de phase du sol.

1 INTRODUCTION

The problem of evaluating the propagation of seismic waves from bedrock, through a soil medium, and predicting the resulting ground motions, is one of the most important problems encountered in geotechnical earthquake engineering. As seismic waves move through soil, they will be influenced by the local conditions as soil can change the frequency content of seismic motion, amplify or attenuate the motion, and change the duration of the motion. Moreover, the soil stratigraphy and layering can complicate the propagation of the seismic waves.

A number of techniques have been proposed to carry out ground response analyses in order to approximate the nonlinear hysteretic stress-strain response of soil during earthquake loading. These analyses may be in one-, two-, or three-dimensional space and are further categorized according to the characteristics of the nonlinear behaviour of the soil mass, and whether or not the interaction of the soil-solid and pore water is considered.

Geotechnical engineering practice has developed three broad classes of soil models to represent cyclic soil behaviour: equivalent linear models, cyclic nonlinear models and advanced constitutive models (Kramer, 1996). Depending on the problem at hand, each of these three models may be a useful representation of soil behaviour for many practical problems.

Advanced constitutive soil models use the principles of mechanics to describe general soil behavior and how strain will occur in response to a given stress increment. Many different types of constitutive models exist with differing levels of complexity and accuracy.

In this paper, the effective stress constitutive model SANISAND described by Dafalias and Manzari (2004) is used to investigate the nonlinear hysteretic stress-strain response of a site subjected to earthquake motions, and the effect of porous-solid and pore water interaction on the seismic site response. For this purpose, one-dimensional effective stress and total stress analyses are carried out to simulate the propagation of nine earthquake input motions recorded on a vertical array of seismographs in Sendai in the Tohoku region of Japan. The vertical array is part of a strong-motion observation network operated by the Port and Airport Research Institute of Japan.

2 CONSTITUTIVE MODEL

SANISAND is the name for a family of Simple ANisotropic SAND constitutive models developed by Manzari and Dafalias (1997), Dafalias and Manzari (2004), Dafalias et al. (2004), Taiebat and Dafalias (2008) and Li and Dafalias (2011). The work by Manzari and Dafalias (1997) represents the core of the constitutive model and the

above-referenced subsequent works build different constitutive features that can be added to the original model framework. The work of Dafalias and Manzari (2004) accounted for fabric change effects of the soil under dilation, a feature that was not initially included in the model formulation of Manzari and Dafalias (1997); this version of SANISAND is used to model soil behavior in the present paper.

The SANISAND constitutive formulation is presented in detail in both triaxial and multiaxial spaces in Manzari and Dafalias (1997) and Dafalias and Manzari (2004). A brief review of the general constitutive formulation is presented in triaxial space here. The constitutive formulation is fully compatible with multiaxial space. Calibration of the model parameters in triaxial space leads to the correct multiaxial implementation (Dafalias and Manzari 2004).

2.1 Basic Concepts and Critical State Framework

SANISAND is based on the concept of a two-surface plasticity formulation, which includes both yield and bounding surfaces. The framework of Critical State Soil Mechanics and stress ratio η form the basis of the SANISAND model (Manzari and Dafalias 1997). Stress ratio is defined as following relation:

$$\eta = \frac{q}{p} \quad [1]$$

where p and q are the mean effective stress and deviatoric stress, respectively.

The critical state is defined as the stress ratio at which soil deformation continues with zero volumetric strain rate (Schofield and Wroth 1968). The stress ratio at critical state is defined as $M = q_c/p_c$, where q_c and p_c are the deviatoric and mean effective stress at critical state, respectively. The stress ratio M is shown as a solid line in triaxial p - q space in Figure 1.

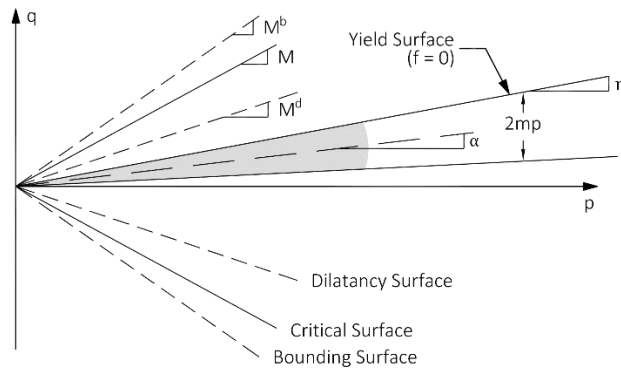


Figure 1. SANISAND model schematic in triaxial p - q space (adapted from Dafalias and Manzari 2004)

At critical state, the critical state void ratio e_c is attained and is defined by the following power relation based on the findings of Li and Wang (1998):

$$e_c = e_0 - \lambda_c \left(\frac{p_c}{p_{at}} \right)^\xi \quad [2]$$

where e_0 is the void ratio at $p_c = 0$, λ_c is the slope of the critical state line, p_{at} is atmospheric pressure, and ξ is a constant. The constant ξ may be assumed to be 0.7 for sands (Li and Wang 2008).

The state parameter ψ introduced by Been and Jefferies (1985) defines the distance between the critical state void ratio e_c and the current void ratio e , and is given by the following relation:

$$\psi = e - e_c \quad [3]$$

2.2 Dilatancy and Bounding Surfaces

The volumetric response of sands will be either dilative or contractive, depending on the stress ratio and whether ψ is positive or negative (i.e. the soil is dense of the critical state or loose of the critical state). A dilatancy surface represented by the dashed line M^d in Figure 1 is used in the SANISAND model to control the volumetric response of soil. For $\eta < M^d$, the soil response is contractive, and for $\eta > M^d$ the soil response is dilative. The dilatancy surface is equivalent to the phase transformation line proposed by Ishihara (1985).

The slope of M^d is variable and approaches critical stress ratio M as the current void ratio approaches e_c . The state parameter ψ relates the dilatancy surface to the critical state stress ratio M by the following equation

$$M^d = M \exp(\eta^d \psi) \quad [4]$$

where η^d is a positive material constant.

Sands may soften prior to reaching critical stress ratio. For example, a sand which is dense of critical and subjected to a drained constant- p triaxial compression tests will first consolidated and then dilate to critical state. The dilation is associated with a softening response which is accounted for in the SANISAND model by the peak stress ratio shown as the bounding surface M^b in Figure 1. Similar to the dilatancy surface, the bounding surface will approach the critical stress ratio M as the current void ratio approaches e_c . The bounding surface is related to the critical stress ratio with the state parameter ψ by the following relation

$$M^b = M \exp(-\eta^b \psi) \quad [5]$$

where η^b is a positive material constant.

Following the logic of Eq. 4 and 5, for $\psi < 0$: $M^d < M < M^b$; for $\psi > 0$: $M^b < M < M^d$, and $M^b = M = M^d$ when $\psi = 0$ (Dafalias and Manzari 2004). This means that M^d and M^b will approach M as ψ approaches zero, and will overlie M at critical state ($\psi = 0$).

2.3 Yield Surface

The yield surface bounds the region wherein stress ratio increments induce only elastic strain and is represented by the following expression

$$f = |\eta - \alpha| - m = 0 \quad [6]$$

where α is the slope of the line bisecting the wedge-shaped yield surface in triaxial p-q space and m defines the opening of the wedge as $2mp$. The yield surface is shown in Figure 1.

2.4 Stress-Strain Relations

Similar to many constitutive models, the SANISAND model strain increments are based on the concept of additive decomposition, and the total strain increment is decomposed into its elastic and plastic parts as follows:

$$\dot{\varepsilon} = \dot{\varepsilon}^e + \dot{\varepsilon}^p \quad [7]$$

where ε represents the strain tensor and the superscripts e and p denote the elastic and plastic parts of strain, respectively. The SANISAND model elastic and plastic strains are represented by the following incremental stress-strain relations:

$$\dot{\varepsilon}_q^e = \frac{\dot{q}}{3G} \quad \dot{\varepsilon}_v^e = \frac{\dot{p}}{K} \quad [8]$$

$$\dot{\varepsilon}_q^p = \frac{\dot{\eta}}{H} \quad \dot{\varepsilon}_v^p = d|\dot{\varepsilon}_q^p| \quad [9]$$

where G and K are the incremental elastic shear and bulk moduli, respectively; H is the plastic hardening modulus; and d is the dilatancy parameter after Rowe's dilatancy theory (Rowe 1962).

The plastic hardening modulus H is defined by the distance between M^b and η , and controls the rate of deviatoric plastic strain. In triaxial p-q space H is defined by the following relation:

$$H = h(M^b - \eta) \quad [10]$$

where h is a positive function of the state variables. The dilatancy parameter d is controlled by the distance between the current stress ratio and the dilatancy surface M^d as shown in the following relation:

$$d = A_d(M^d - \eta) \quad [11]$$

where A_d is a function of the state variables.

Based on the work of Richart et al. (1970) and Li and Dafalias (2000), the mean effective stress and current void ratio e determine the incremental G, which can be expressed as:

$$G = G_0 p_{at} \frac{(2.97 - e)^2}{1 + e} \left(\frac{p}{p_{at}} \right)^{1/2} \quad [12]$$

where G_0 is a constant and p_{at} is the atmospheric pressure for normalization.

3 NUMERICAL PLATFORM AND CONTINUUM MODEL

The OpenSees (Open System for Earthquake Engineering Simulation) finite element program developed

by McKenna and Fenves (2001) was used to carry out the nonlinear site response analyses. OpenSees is open-source software which contains a large number of independent libraries of elements, constitutive models, solution algorithms, equation solvers and integrators. OpenSees is an object-oriented framework and includes a set of modules which create the finite element domain, specify analysis procedures, monitor quantities during analysis, and provide the results (Mazzoni et. al. 2007).

The ground response analyses were completed to simulate one-dimensional seismic wave propagating through total and effective stress model configurations. The analyses all consider a generic 10 m thick layer of sand represented by the SANISAND constitutive model implemented in OpenSees, overlying an elastic half space. The groundwater table is located at 2 m below the surface. A parabolic distribution of shear wave velocity V_s in the sand was assumed to be between 120 and 300 m/s, from the surface to the base of the model. The ground response models were adapted from examples of total and effective stress ground response analyses prepared by McGann and Arduino (2011), available on the OpenSees website (opensees.berkeley.edu). A general schematic of the site stratigraphy and shear wave velocity distribution is illustrated in Figure 2.

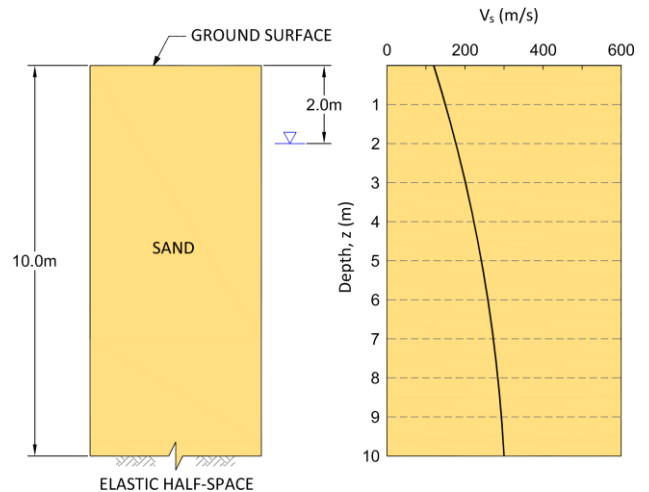


Figure 2. Schematic of site stratigraphy and shear wave velocity

The effective and total stress analyses were completed using the same model dimensions and configuration, constitutive material, loading pattern and equation solvers. Boundary conditions applied to the two models were also the same for the displacement degrees-of-freedom. Different element types were used in the two analyses. The bulk soil mass density was used to establish the in situ at rest stress conditions in the effective stress analyses, whereas the submerged soil mass density was used in the total stress analyses.

Four-node SSPquad and SSPquadUP elements with plane strain formulation were used for the total stress and effective stress analyses, respectively. Both elements use physical hourglass stabilization techniques to facilitate using only one integration point at the center and also to

prevent instability at the incompressible-impermeable limit. An extension of the work of Biot (1944) by Zienkiewicz and Shiomi (1984) is used for the mixed displacement-pressure (u-p) formulation to predict the development of pore water pressures in the SSPquadUP element (McGann et al. 2012). The minimum vertical element size was selected to be 0.25 m in order to allocate eight elements to a wavelength propagating with a maximum frequency of $f_{max} = 50$ Hz. through soil with a minimum shear wave velocity $V_{s-min} = 120$ m/s.

To model the elastic half-space underlying the site, a Lysmer-Kuhlemeyer dashpot (Lysmer and Kuhlemeyer 1969) is used at the base of the model. The dashpot is modeled using a viscous uniaxial constitutive material and a zeroLength element type is connected to a single node at the base of the column. The dashpot coefficient is determined following the method of Joyner and Chen (1975).

4 EARTHQUAKE INPUT MOTIONS

Nine earthquake records from the Sendai station of the Port and Airport Research Institute seismograph network were used as input motions for the nonlinear site response analyses. The east-west components of the recorded motions were applied as velocity time histories at the base of the model. The depth that input motions were applied in the analyses (10 m) is near the depth that the motions were recorded, and therefore the motions were applied as rigid base motions. No attempt was made to simulate the actual ground conditions at the vertical array as part of this work.

A summary of the earthquake motions and their moment magnitude M_w , epicentral distance from the vertical array, horizontal peak ground acceleration (PGA) at the downhole seismograph, and duration is provided in Table 1.

Table 1. Summary of real input ground motions

Time Series	PGA (g)	Duration (sec)
TS1100	0.251	312
TS2100	0.063	136
TS3100	0.062	106
TS4100	0.025	141
TS5100	0.026	110
TS6100	0.036	156
TS7100	0.012	78
TS8100	0.005	78
TS9100	0.003	78

The motion TS1100 is the recorded motion during the 2011 M_w 9.0 Tohoku earthquake. This motion was scaled by constant factors of 0.5 (TS1050), 0.75 (TS1075), 1.25 (TS1125) and 1.5 (TS1150), and the resulting time histories were applied as additional artificial input motions to the model to cover a range of PGAs. A summary of the artificial scaled motions is provided in Table 2.

Table 2. Summary of artificial input ground motions

Time Series	PGA (g)	Duration (sec)
TS1050	0.125	312
TS1075	0.189	312
TS1125	0.314	312
TS9100	0.376	312

5 CONSTITUTIVE MODEL PARAMETERS

The SANISAND model parameters for Toyoura Sand were selected for the nonlinear analyses based on the model validation by Taiebat et al. (2010), who compared experimental results and numerical simulations for different types of sand. The model parameters are summarized in Table 3.

Table 3. SANISAND Model Parameters for Toyoura Sand (adapted from Taiebat et al. 2010)

Parameter	Symbol	Value
Elasticity	G_0	Variable ¹
	N	0.05
Critical state line	M	1.25
	C	0.712
	e_0	0.934
	λ	0.019
Dilatancy	ξ	0.7
	n^d	2.1
	A_0	0.704
Kinematic	n^b	1.25
	Hardening	h_0
C_h		0.968
Fabric dilatancy	Z_{max}	2.0
	C_z	600

¹see Table 4 for G_0 values

The small strain shear modulus determined in the laboratory and by in situ measurements can differ greatly (Ishihara 1996). This difference effects the calibration of the model constant G_0 . It is the writers' experience that when the SANISAND G_0 model constant is calibrated against conventional triaxial laboratory data, the resulting G_0 value can be a factor lower than required to model in situ soil stiffness. This can result in the fundamental period of the modeled site being shifted to larger periods which is not realistic. Therefore, the SANISAND model for this research is calibrated at 1 m intervals over the depth of the model based on the in situ shear wave velocity, confining pressure and void ratio using Eq. 10. The G_0 model constant values are summarized in Table 4.

Table 4. SANISAND G_0 model constant values

Depth (m)	Value
0 - 1	365
1 - 2	370
2 - 3	435
3 - 4	490
4 - 5	535
5 - 6	580
6 - 7	620
7 - 8	660
8 - 9	700
9 - 10	740

The initial void ratio e_i of the site is selected to be $e_i = 0.73$ to simulate Toyoura Sand with a relative density of 65%, based on the maximum and minimum void ratios for Toyoura Sand provided in Ishihara (1996). The mass density ρ of the modeled sand is $\rho = 1700 \text{ kg/m}^3$. The soil permeability in the effective stress analyses is selected to be $k = 10^{-5} \text{ m/s}$.

6 COMPARISON OF EFFECTIVE AND TOTAL STRESS ANALYSES

The horizontal input motion PGAs at the base of the model and the computed horizontal PGAs at the surface of the model for each of the nine time series are presented in Figure 3 for both the effective and total stress nonlinear site response analyses.

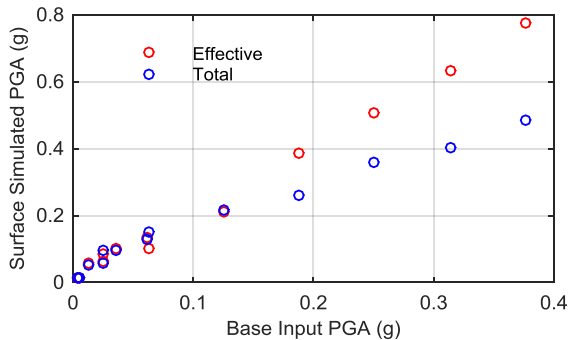


Figure 3. Comparison of surface horizontal PGAs computed with effective and total stress analyses

The computed horizontal PGAs at the surface of the effective and total stress models are reasonably similar for the base input PGAs up to 0.125 g (TS1050). However, the horizontal surface PGA computed using the effective and total stress models diverge with the base input PGA of 0.189 g (TS1075), with a difference of 0.13 g between the two models.

The spectral acceleration S_a responses for both the effective and total stress models are illustrated for TS1100 and TS6100 in Figures 4 and 5, respectively. The TS1100 and TS6100 time series are selected to illustrate representative site response to relatively weak input motion (i.e. TS6100) and strong input motion (i.e. TS1100).

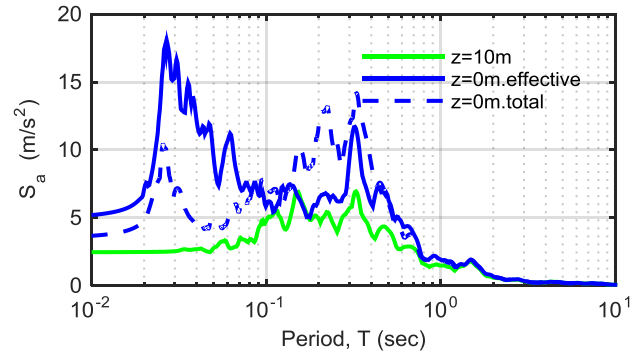


Figure 4. Spectral acceleration response for TS1100 at the base ($z=10\text{m}$) and surface ($z=0\text{m}$) of the model

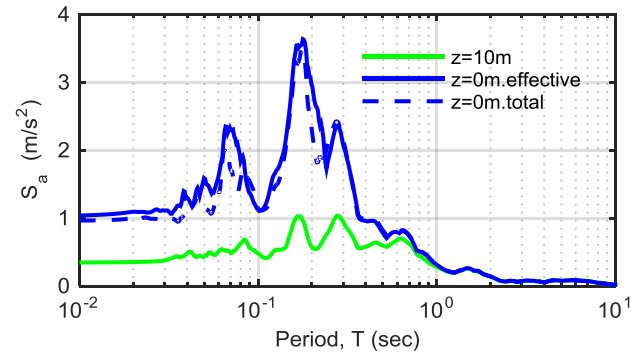


Figure 5. Spectral acceleration response for TS6100 at the base ($z=10\text{m}$) and surface ($z=0\text{m}$) of the model

The S_a plots in Figures 4 and 5 show that TS6100 with a peak input PGA of 0.036 g has a very similar response for both the effective and total stress analyses. However, the difference between effective and total stress S_a response is pronounced for TS1100, with the response changing generally over the period (T) range of interest as follows: $T < 0.09$ seconds (short period range) $\rightarrow S_a \text{ effective} > S_a \text{ total}$; $0.09 < T < 0.5$ seconds (short to intermediate period range) $\rightarrow S_a \text{ effective} < S_a \text{ total}$; $T > 0.5$ seconds $\rightarrow S_a \text{ effective} \approx S_a \text{ total}$.

To further explore the difference between the TS1100 effective and total stress S_a responses, the acceleration response time history and pore pressure coefficient r_u corresponding to a site depth between 7 and 8 m are plotted for the TS1100 and TS6100 effective stress analyses in Figures 6 and 7.

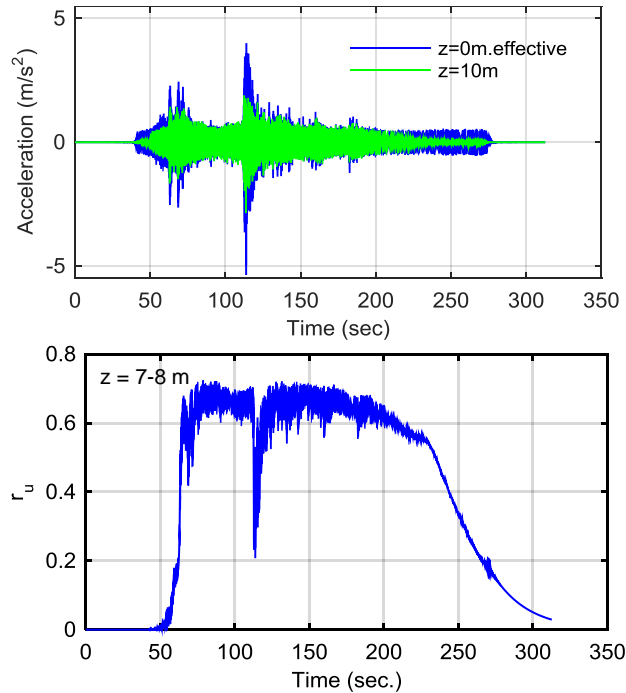


Figure 6. Time history and r_u for TS1100 effective stress analysis between 7 and 8 m depth

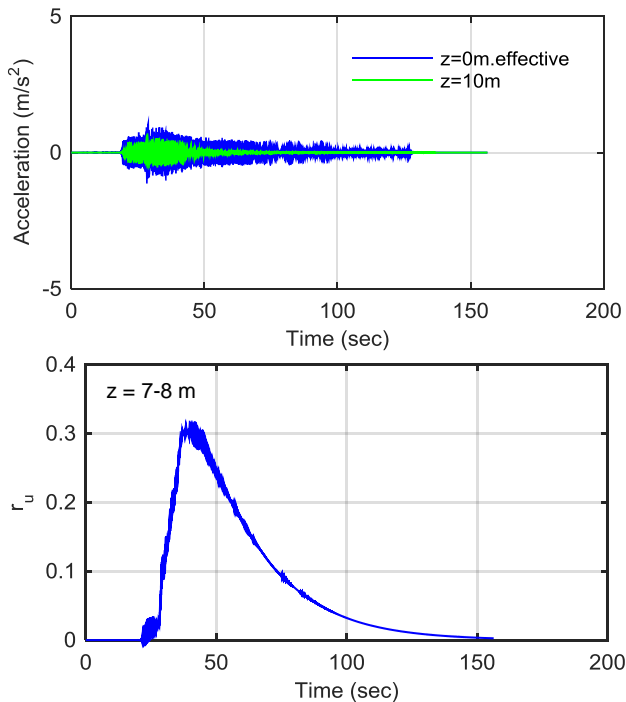


Figure 7. Time history and r_u for TS6100 effective stress analysis between 7 and 8 m depth

For the smaller input motion TS6100, the r_u value starts building up at the onset of earthquake motion to a maximum value of approximately 0.3, followed by a

gradual drop as the excess pore water pressure dissipates.

The acceleration time history for TS1100 in Figure 6 shows that at approximately 112 seconds, the amplitude of the input acceleration at the base of the model increases, corresponding with an approximately 40% drop in the pore pressure coefficient for TS1100; relating to a drop in excess pore pressure from approximately 48 kPa to 19 kPa. The spikes in the simulated acceleration time history at the surface ($z=0m$) at approximately 112 seconds are proposed to be caused by a strain stiffening shear modulus associated with a drop in excess pore pressure caused by soil dilatancy when the stress path begins to cross the phase transformation line identified by Ishihara (1985). This behaviour is contrary to the shear modulus reduction curves often used for the calibration of soil models in seismic site response analyses, as soil dilatancy at increased levels of strain results in a stiffening shear modulus (Kutter and Wilson 1999).

The simulated stress path is plotted as shear stress τ against vertical effective stress σ_v' between 7 and 8 m depth during TS1100 and TS6100 earthquake loading in Figures 8 and 9, respectively.

The TS1100 stress path is filtered between 112.47 and 121.85 seconds in Figure 7 to highlight the site response during the sudden drops and increases in r_u as the soil changes between contractive and dilative behaviour associated with the stress path crossing the phase transformation line. No dilative soil response is observed from the TS6100 simulated stress path.

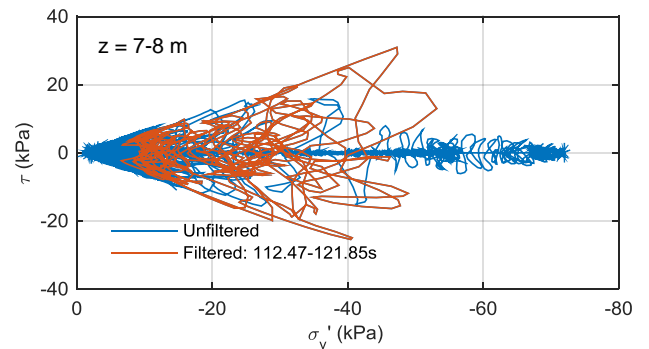


Figure 8. Stress path between 7 and 8 m depth during TS1100 loading

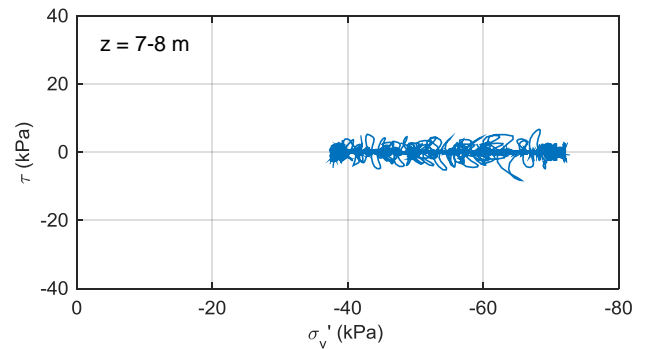


Figure 9. Stress path between 7 and 8 m depth during TS6100 loading

Kutter and Wilson (1999) proposed the term “de-liquefaction shock waves” to describe soil stiffening due to dilatancy and identified this as a source of high-frequency acceleration pulses. Kramer et al. (2015) later referred to soil stiffening due to dilatancy as dilation pulses. To link the TS1100 simulated high frequency response with dilative soil behaviour, the response spectra for TS1100 is plotted for different periods of the time history in Figure 10.

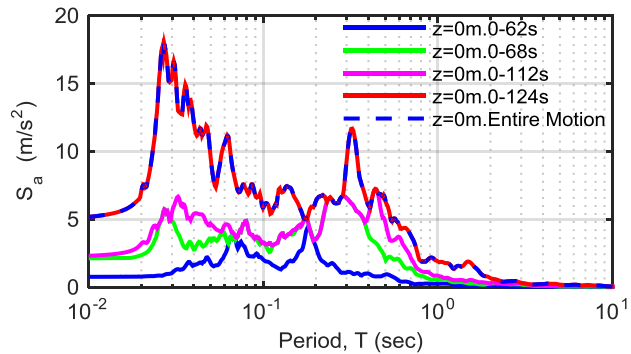


Figure 10. Response spectra for TS1100 at 62, 68, 112, 124s and for the entire motion

The low period (high frequency) content of the response spectra for TS1100 in Figure 10 can be seen to increase with time up until 124 seconds, after which the response spectra for the entire motion is nearly identical to that of spectra at 124 seconds. The response spectra at 112 seconds (just before the onset of significant soil dilation) has less high frequency content than the response spectra at 124 seconds, indicating that the simulated high frequency response is primarily associated with soil dilative behaviour between 112 and 124 seconds. Some less significant soil dilative behaviour, and resulting high frequency ground motion, also occurs between 62 and 68 seconds, which is observed by comparing the response spectra at these two times.

Soil dilation was identified as the source of high frequency motion at Onahama Port near Iwaki, Japan during the 2011 Tohoku M_w 9.0 earthquake by Roten et al. (2013). High-frequency ground amplification appears to be particularly important when shallow soft surface soil layers are considered (Finn and Ruz 2015). The analyses presented here point towards the SANISAND model as being capable of reproducing high frequency ground motion associated with soil dilation.

7 CONCLUSIONS

The SANISAND constitutive model implemented in OpenSees was used to investigate the effective and total stress nonlinear response of a shallow sand site subjected to seismic loading.

The influence of modeling the soil-solid and pore water fluid interaction in the effective stress analyses was

shown to be significant for the dynamic response of soil to earthquake motions with increasing PGA. In general, the total and effective stress analyses provided similar predictions of ground response when the model was subjected to input ground motions with lower PGAs (TS2100 through TS9100). However, the difference between the total and effective stress computed motions became more significant as the ground motion intensity increased (TS1050 through TS1150).

Modeling the solid-pore fluid interaction during the seismic response analysis of a 10 m deep site was shown to be particularly important when medium dense sands may be subject to cyclic mobility and a strain-stiffening response during earthquake loading, resulting in soil dilation and high frequency acceleration pulses. This type of behaviour is consistent with recent observations of increased ground amplification at frequencies above 10 Hz. during the 2011 Tohoku earthquake (Roten et al. 2013). Soil dilative behaviour and a strain-stiffening response was inferred to govern the simulated PGA as ground motion intensity increased. This is in contrast to the conventional shear modulus reduction curves commonly used for the calibration of nonlinear soil models which are based on the soil shear modulus reducing with increasing levels of strain (Kutter and Wilson 1999).

The total stress analysis for TS1100 was unable to capture the high frequency motion as a result of dilative soil behaviour using the model applied in this research. Consequently, the total stress analysis underestimates the horizontal PGA at the surface of the site.

The effective stress application of the SANISAND model for the prediction of ground motions during an earthquake event may be able to provide a more realistic method of carrying out site response analyses when soil-solid and pore-water interaction significantly impact the predicted ground behaviour. The SANISAND model appears to be capable of capturing high frequency soil dilative behaviour.

ACKNOWLEDGEMENTS

Support to conduct this study is provided by grant from the Natural Sciences and Engineering Research Council of Canada (NSERC) and Levelton Consultants Ltd. The writers would like to acknowledge the contribution Mr. Doug Wallis for his technical input into this paper. The strong motion records were obtained from the Port and Airport Research Institute (<http://www.eq.pari.go.jp/kyosin/>).

REFERENCES

- Been, K., and Jefferies, M.G. 1985. A state parameter for sands, *Geotechnique*, 35(2): 99-112.
- Biot, M.A. 1958. Theory of propagation of elastic waves in a fluid-saturated porous solid, *The Journal of the Acoustical Society of America*, 28(2): 168-178.
- Dafalias, Y.F., and Manzari, M.T. 2004. Simple plasticity sand model accounting for fabric change effects, *Journal of Engineering Mechanics*, 36(1): 65 - 78.

- Dafalias, Y.F., Papadimitriou, A.G., and Li, X.S. 2004. Sand plasticity model accounting for inherent fabric anisotropy, *Journal of Engineering Mechanics*, 130(11): 1319-1333.
- Finn, W.D.L., and Ruz, F. 2015. Amplification effects of thin soft surface layers: a study for NBCC 2015, *Perspectives in Earthquake Geotechnical Engineering*, Springer International Publishing, 33-44.
- Ishihara, K. 1996. Oxford University Press, New York, NY, USA.
- Ishihara, K. 1985. Stability of natural deposits during earthquakes, *Proceedings of the 11th International Conference on Soil Mechanics and Foundation Engineering*, 1: 321-376.
- Joyner, W.B., and Chen, A.T.F. 1975. Calculation of nonlinear ground response in earthquakes, *Bulletin of Seismological Society of America*, 65(5): 1315-1336.
- Kramer, S.L. 1996. *Geotechnical earthquake engineering*, Prentice-Hall, Upper Saddle River, NJ, USA.
- Kramer, S.L., Asl, B.A., Ozener, P., and Sideras, S.S. 2015. Effects of liquefaction on ground surface motions. *Perspectives in Earthquake Geotechnical Engineering*, Springer International Publishing, 285-309.
- Kutter, B.L., and Wilson, D.W. 1999. De-liquefaction shock waves, *Proceedings of the 7th U.S.-Japan Workshop on Earthquake Resistant Design for Lifeline Facilities and Countermeasures Against Soil Liquefaction*, Technical Report MCEER-99-0019 (O'Rourke, Bardet, and Hamada eds.), 295-310.
- Li, X.S., and Dafalias, Y.F. 2011. Anisotropic critical state theory: role of fabric, *Journal of Engineering Mechanics*, 138(3): 263-275.
- Li, X.S., and Wang, Y. 1998. Linear representation of steady-state line for sand, *Journal of Geotechnical and Geoenvironmental Engineering*, 124(12): 1215-1217.
- Li, X.S., and Dafalias, Y.F. 2000. Dilatancy of cohesionless soils, *Geotechnique*, 50(4): 449-460.
- Lysmer, J., and Kuhlemeyer, A.M. 1969. Finite dynamic model for infinite media, *Journal of Engineering Mechanics*, ASCE, 95: 859-877.
- Mazzoni, S., McKenna, F., Scott, M.H., Fenves, G.L. 2007. *The OpenSees command language manual*, Pacific Engineering Research Center, University of California, Berkeley, CA, USA.
- Manzari, M.T., and Dafalias, Y.F. 1997. A critical state two-surface plasticity model for sands, *Geotechnique*, 47(2): 255-272.
- McGann, C. and Arduino, P. 2011. *Site response analysis of a layered soil column (total stress analysis)*, <http://opensees.berkeley.edu>.
- McGann, C.R., Arduino, P., and Mackenzie-Helnwein, P. 2012. Stabilized single-point 4-node quadrilateral element for dynamic analysis of fluid saturated porous media, *Acta Geotechnica*, 7(4): 297-311.
- McKenna, F. and Fenves, G.L. 2001. *The OpenSees command language manual, Version 1.2*, Pacific Engineering Research Center, University of California, Berkeley, CA, USA.
- Richart, F.E., Jr., Hall, J.R., and Woods, R.D. 1970. Vibration of soils and foundations, *International Series in Theoretical and Applied Mechanics*, Prentice-Hall, Englewood Cliffs, NJ, USA.
- Roten, D., Fah, D., and Bonilla, L.F. 2013. High-frequency ground motion amplification during the 2011 Tohoku earthquake explained by soil dilatancy, *Geophysical Journal International*, 193(2): 898-904.
- Rowe, P.W. 1962. The stress-dilatancy relation for static equilibrium of an assembly of particles in contact, *Proceedings of the Royal Society of London, Series A*, 269: 500-527.
- Schofield, A.N., and Wroth, C.P. 1968. *Critical state soil mechanics*, McGraw-Hill, New York, NY, USA.
- Taiebat, M., and Dafalias, Y.F. SANISAND: simple anisotropic sand plasticity model, *International Journal of Numerical and Analytical Methods in Geomechanics*, 32(8): 915-948.
- Taiebat, M., Jeremic, B., Dafalias, Y.F., Kaynia, A.M., and Cheng, Z. 2010. Propagation of seismic waves through liquefied soils. *Soil Dynamics and Earthquake Engineering*, 30(4): 236-257.
- Zienkiewicz, O.C., and Shiomi, T. 1984. Dynamic behaviour of saturated porous media; the generalized Biot formulation and its numerical solution, *International Journal of Numerical Methods in Engineering*, 8(1): 71-96.